MCB
Journals.ASM.org

RNA Binding Protein Ptbp2 Is Essential for Male Germ Cell Development

Leah L. Zagore,[a,b] Sarah E. Grabinski,[a] Thomas J. Sweet,[a*] Molly M. Hannigan,[a,b] R. Michael Sramkoski,[c] Qin Li,[d] Donny D. Licatalosi[a,b]

Center for RNA Molecular Biology,[a] Department of Biochemistry,[b] and Case Comprehensive Cancer Center,[c] Case Western Reserve University, Cleveland, Ohio, USA; Department of Microbiology, Immunology, and Molecular Genetics, University of California, Los Angeles, Los Angeles, California, USA[d]

RNA binding proteins (RBPs) are increasingly recognized as essential factors in tissue development and homeostasis. The polypyrimidine tract binding (PTB) protein family of RBPs are important posttranscriptional regulators of gene expression. In the nervous system, the function and importance of PTB protein 2 (Ptbp2) as a key alternative splicing regulator is well established. Ptbp2 is also abundantly expressed during spermatogenesis, but its role in this developmental program has not been explored. Additionally, the importance of alternative splicing regulation in spermatogenesis is unclear. Here, we demonstrate that Ptbp2 is essential for spermatogenesis. We also describe an improved dual fluorescence flow cytometry strategy to discriminate, quantify, and collect germ cells in different stages of development. Using this approach, in combination with traditional histological methods, we show that Ptbp2 ablation results in germ cell loss due to increased apoptosis of meiotic spermatocytes and postmeiotic arrest of spermatid differentiation. Furthermore, we show that Ptbp2 is required for alternative splicing regulation in the testis, as in brain. Strikingly, not all of the alternatively spliced RNAs examined were sensitive to Ptbp2 loss in both tissues. Collectively, the data provide evidence for an important role for alternative splicing regulation in germ cell development and a central role for Ptbp2 in this process.

Tissue-restricted RNA binding proteins (RBPs) have central roles in posttranscriptional regulatory events necessary for tissue development and the specialization of cell functions. Through interactions with nascent transcripts, RBPs can impact alternative splicing and polyadenylation, two highly regulated processes that permit genes to generate multiple RNA isoforms with different combinations of coding and noncoding sequences. Further proteome diversity and control are imparted by RBPs that act on mature mRNAs to alter stability and translation. Accordingly, changes in the levels/activity of specific RBPs underlie key transcriptome and proteome remodeling events that drive multiple developmental pathways (1, 2).

The polypyrimidine tract binding (PTB) proteins are among a group of multifunctional RBPs that have key roles in tissue-specific posttranscriptional programs (3–5). While Ptbp1 is expressed in most tissues, Ptbp2 (also called brain or neuronal PTB protein [br/nPTB]) is more tissue restricted, with high levels of expression in brain and testis (6–8). Despite their high sequence similarity, Ptbp1 and Ptbp2 regulate the alternative splicing (AS) of overlapping but nonredundant sets of mRNA targets, with some AS exons more strongly repressed by one PTB protein paralog than the other (9–12). Accordingly, a switch in PTB protein expression from Ptbp1 to Ptbp2 is associated with changes in the expression of AS isoforms during neuronal differentiation (9, 10). Ptbp2 is an essential AS factor in the developing nervous system, where it has a prominent role in repressing AS exons that are enriched in the adult brain (13, 14). While PTB proteins have been extensively studied in nervous system development, the requirements and role(s) of PTB proteins in the testis have not been explored.

The testes are packed with seminiferous tubules where postnatal male germ cell development (spermatogenesis) occurs. In the first stage of spermatogenesis, spermatogonial stem cells self-renew to maintain the germ line stem cell pool. They also generate undifferentiated spermatogonia that undergo multiple rounds of mitotic division and differentiation prior to entering meiosis (15). In the meiotic stage of spermatogenesis, a prolonged prophase is followed by two relatively quick cellular divisions to yield haploid round spermatids. In the third stage of spermatogenesis (spermiogenesis), spermatids undergo dramatic morphological changes to become spermatozoa that are released into the seminiferous tubule lumen (16, 17). Throughout spermatogenesis, germ cells have extensive contact and communication with Sertoli cells, the somatic cell type that physically spans the seminiferous epithelium. Sertoli cells provide structural and nutritional support to germ cells via specialized cell-cell junctions that are continuously assembled and disassembled as germ cells translocate from the basal surface of the seminiferous tubule to the lumen (18).

The mammalian testis ranks among the top tissues with respect to transcriptome complexity, expressing the most genes (~84%) and AS RNA isoforms (19, 20). While the importance of mRNA translational control in spermatogenesis is well established (for a review, see reference 21), the functional significance of the high levels of AS in the testis is unclear. The roles and regulation of AS in spermatogenesis are also not well understood.

Received 6 July 2015 **Returned for modification** 10 August 2015
Accepted 14 September 2015

Accepted manuscript posted online 21 September 2015

Citation Zagore LL, Grabinski SE, Sweet TJ, Hannigan MM, Sramkoski RM, Li Q, Licatalosi DD. 2015. RNA binding protein Ptbp2 is essential for male germ cell development. Mol Cell Biol 35:4030–4042. doi:10.1128/MCB.00676-15.

Address correspondence to Donny D. Licatalosi, ddl33@case.edu.

* Present address: Thomas J. Sweet, Genomic Medicine Institute, Lerner Research Institute, Cleveland Clinic Foundation, Cleveland, Ohio, USA.

Multiple RBPs with known roles in AS regulation are differentially expressed in different stages of germ cell development, including members of the SR, hnRNP, MBNL, and CELF families of RBPs (21–23). Reminiscent of the largely nonoverlapping expression observed in the nervous system (9, 10), the relative levels of the PTB proteins differ in different stages of spermatogenesis. Ptbp1 is the predominant isoform in mitotic cells (spermatogonia), while Ptbp2 predominates in meiotic spermatocytes and postmeiotic spermatids (22, 24). Little to no Ptbp2 is present in somatic cells of the testes, as indicated by immunohistochemical analyses (24, 25). Due to a more open chromatin state, the majority of the genome is transcribed in spermatocytes and spermatids (20). It is unclear whether the increase of Ptbp2 signifies important roles for this RBP in the meiotic and postmeiotic stages of spermatogenesis or is an indirect and inconsequential result of widespread promiscuous transcription.

In this study, we investigated the requirements and roles of Ptbp2 in mouse spermatogenesis. Using a Cre-lox system to delete Ptbp2 in the postnatal testis, we demonstrate that Ptbp2 is an essential spermatogenic factor. Histological examination showed that Ptbp2 loss resulted in complete arrest in the early stages of postmeiotic cell differentiation, concomitantly with premature release of spermatids into the lumen. In parallel, we used an original dual fluorescence flow cytometry strategy to discriminate and quantify germ cells in each of the major stages of spermatogenesis. Applying this method to the analysis of Ptbp2-null germ cells uncovered a second, partial spermatogenic block during meiosis I, manifested by increased spermatocyte apoptosis. Altogether, the phenotypic features of Ptbp2-null germ cells suggest important roles for Ptbp2 in germ cell contact and communication with Sertoli cells.

Additionally, examination of a subset of AS RNAs that are regulated by Ptbp2 in the brain confirmed that Ptbp2 is also required for proper AS regulation in the testis. Strikingly, not all of the RNAs examined were regulated by Ptbp2 in both the brain and testis. Collectively, these findings demonstrate that Ptbp2 is required for spermatogenesis and that testis-specific AS regulation may have essential roles in the meiotic and postmeiotic stages of mammalian spermatogenesis.

MATERIALS AND METHODS

Animals and tissue collection. Mice bearing the *Stra8-iCre* transgene [stock Tg(Stra8-icre)1Reb/J] and the *IRG* transgene (B6.Cg-Tg[CAG-DsRed,-EGFP]5Gae/J) were purchased from The Jackson Laboratory (Bar Harbor, ME). C57BL6 mice bearing $Ptbp2^{flox}$ were generously provided by Qin Li and Douglas Black (UCLA). Mice bearing the $Ptbp2^{+/pDLTV1}$ allele used for timed matings and embryonic brain collection were previously described (13). For all procedures, mice were sacrificed by isoflurane inhalation followed by cervical dislocation or decapitation. Testes were detunicated in Gey's balanced salt solution (GBSS) (Sigma). All animal procedures were approved by the Institutional Animal Care and Use Committee at Case Western Reserve University (CWRU).

Histology. Epididymides and decapsulated testes were fixed overnight at 4°C in 4% paraformaldehyde and then washed in phosphate-buffered saline (PBS) prior to paraffin embedding by the Histology Core Facility at CWRU. Slides containing 5-μm sections were deparaffinized in xylene (3 times for 5 min each), followed by a 1-min rinse in 100% ethanol. Slides were rehydrated by 30-s incubations in 100%, 95% (twice), and 80% ethanol, followed by a 2-min rinse with tap water.

For hematoxylin and eosin staining, slides were incubated with Harris modified hematoxylin (Fisher Scientific) for 7 min and then rinsed in tap water for 1 min. The tissue was differentiated for 30 s in 0.3% acid alcohol with agitation, followed by a 1-min rinse in tap water to halt destaining. Slides were then submerged in saturated lithium carbonate 3 to 6 times until tissue became blue and then rinsed with tap water for 1 min. For eosin counterstaining, slides were washed with 95% ethanol for 1 min, stained with 0.0625% eosin Y (Sigma) for 30 s, and then differentiated for 30 s in 95% ethanol with agitation. Slides were then washed with 100% ethanol for 30 s (3 times) and xylene for 1 min prior to mounting coverslips with Acrymount mounting media.

For periodic acid-Schiff-hematoxylin (PASH) staining, deparaffinized and rehydrated slides were incubated with 1% periodic acid for 30 s and then washed for 1 min with tap water. Slides were then incubated with Schiff's reagent for 5 min, followed by a 5-min rinse with tap water. Slides were subsequently stained with hematoxylin, dehydrated, and mounted with coverslips (as described above).

Terminal deoxynucleotidyltransferase-mediated dUTP-biotin nick end labeling (TUNEL) staining was performed using reagents from the Roche TUNEL kit. Deparaffinized slides were equilibrated in PBS and permeabilized with 0.02 mg/ml proteinase K solution (in 10 mM Tris, pH 7.4) for 15 min at room temperature. TUNEL mix (1:10) was added to slides and incubated for 1 h at 37°C in a humidified chamber. After a PBS rinse, converter peroxidase (POD) was added to each slide followed by a 30-min incubation at 37°C in a humidified chamber. Slides were then rinsed in PBS. 3,3′-Diaminobenzidine (DAB) substrate was prepared by combining 10 ml PBS with 500 μl DAB (Sigma) and 500 μl H_2O_2 and adjusting the pH to ~7.4 with 1 N NaOH. DAB substrate was added to slides for 30 s to 1 min and then rinsed in PBS. Slides were then dehydrated for 30 s in 100% ethanol (three times) and 1 min in xylene (two times) prior to mounting coverslips with Acrymount mounting medium. All images were captured using an Olympus BX41T microscope and a SPOT-idea 5-MP digital camera.

Isolation and flow cytometry analysis of seminiferous epithelial cells. To dissociate and stain seminiferous tubule cells with Hoechst 33422 (Ho), we developed a modified strategy based on previously described protocols (26–32). Both testes from each animal were decapsulated in cold GBSS (Sigma) and pooled into a 15-ml conical tube containing 3 ml prewarmed (33°C) single-cell suspension buffer (GBSS containing 120 U/ml collagenase type I [Worthington Biochemical]). Following the addition of 10 μl 1-mg/ml DNase I (in 50% glycerol) and gentle shaking to initiate the dissociation of seminiferous tubules, the tubes were placed horizontally at 33°C for 10 min at 120 rpm. The supernatant containing interstitial cells was removed, and the collagenase digestion was repeated. Settled tubules were then resuspended in 2.5 ml of 33°C single-cell suspension buffer containing 10 μl DNase I and 50 μl of 50 mg/ml trypsin (Worthington Biochemical). Tubes were mixed by gentle inversion and placed horizontally at 33°C for 15 min at 120 rpm. Seminiferous tubules were then disrupted with a wide-mouth pipette for 3 min. After the addition of 30 μl trypsin and 10 μl DNase I, tubes were again mixed by gentle inversion and placed horizontally at 33°C for 15 min at 120 rpm. To inactivate trypsin, 400 μl of prewarmed (33°C) filter-sterilized fetal calf serum (Life Technologies) was added. Cells were then pelleted by centrifugation for 5 min at 500 relative centrifugal force (RCF) at room temperature and resuspended in 3 ml prewarmed incomplete Hanks balanced salt solution (HBSS) containing 10 μl DNase I. Cells were counted on a hemocytometer, and 5 μg Hoechst 33342 (in dimethyl sulfoxide [DMSO; Sigma]) was added per million cells. The cells were then incubated at 33°C for 30 min at 120 rpm while being shielded from light. Using a wide-mouth pipette, the single-cell suspension was then filtered through two 40-μm cell strainers that were stacked and prewetted with incomplete HBSS. Five microliters propidium iodide (PI) and 10 μl DNase were added to the flowthrough, and the cell suspension was kept on ice in the dark until ready for sorting.

Cell analysis and sorting were performed on a Reflection highly automated parallel sort (HAPS) module (Sony Biotechnology Inc.) equipped with a 150-mW Xcyte 355-nm UV laser (JDS Uniphase Corp.) and a 488- to 500-nm argon-ion sapphire laser (Coherent Inc.) which was split to deliver 250 mW to the HAPS module. The Reflection has two beam paths,

with the first being the 488-nm laser and the second containing the UV laser. Green fluorescent protein (GFP) was excited by the 488-nm laser, and the emitted light was acquired with a 525/50 band pass. Hoechst 33342 and PI were excited by the UV laser with Hoechst emission acquired with a 455/50 band pass (Hoechst blue) and a 665/30 band pass (Hoechst red). WinList 3D (version 7.0; Verity Software House Inc.) was used on the Reflection for data acquisition and establishing sorting gates.

Protein isolation and Western blotting. Seminiferous tubules were mechanically disrupted in 1.5-ml tubes containing lysis buffer (150 mM NaCl, 20 mM Tris-HCl, pH 8.0, 1.0% Triton X-100, 0.1% SDS, and Complete EDTA-free protease inhibitor [Roche]) using a plunger from a 1-ml syringe. After complete tissue disruption, the lysate was centrifuged in polycarbonate tubes (Beckman) for 20 min at 30,000 rpm at 4°C. Supernatants were transferred to new tubes, and protein concentrations were determined using Bradford reagent (Bio-Rad). For Western blot analyses, the following primary antibodies were used: anti-Ptbp2 (7), anti-Dazl (Abcam), anti-Hsp90 (BD Biosciences), anti-red fluorescent protein (anti-RFP) (Abcam), and anti-GFP (Santa Cruz Biotech).

RNA isolation and analyses. Seminiferous tubules were homogenized in 1 ml of Ribozol (Amresco) in 1.5-ml tubes using a plunger from a 1-ml syringe. Following the addition of 200 μl of chloroform, samples were mixed by inversion and centrifuged for 15 min at 12,000 RCF at 4°C. Supernatants were transferred to new tubes, and RNA was precipitated by the addition of 500 μl isopropanol and centrifugation for 10 min at 12,000 RCF at 4°C. The resulting pellets were washed with 75% ethanol and centrifuged for 5 min at 7,500 RCF at 4°C. After air drying, pellets were resuspended in 100 μl of water, followed by the addition of 350 μl of RLT buffer (Qiagen) containing β-mercaptoethanol and the addition of 250 μl of ethanol. Samples were then applied to RNeasy spin columns (Qiagen), and on-column DNase digestion, washes, and elution steps were performed according to the manufacturer's instructions. For isolation of RNA from sorted cells, RNeasy minikits were used (Qiagen). First-strand cDNA synthesis was performed with SuperScript III (Invitrogen) and random hexamers. Quantitative reverse transcription-PCR (RT-PCR) was performed with SYBR green master mix (Life Technologies) using a StepOne real-time PCR system (Applied Biosystems). All reactions were performed using technical and biological replicates and normalized to β-actin levels. RT-PCR analysis of alternatively spliced transcripts was performed as previously described (13). The following primers were used: *Pgk2* (forward, ACTTGCTTCCTGTTTCCTGC; reverse, GATGGCTCA CTGCTAGCTCA), *Actb* (forward, TCGTGCGTGACATCAAAGAGA; reverse, GAACCGCTCGTTGCCAATAGT), *Rhox13* (forward, ACCCAG TACCCGGATTTGCTTACA; reverse, TCTGCTTCGCTCTCCGATTGG TAA), *Dazl* (forward, TTCAGGCATATCCTCCTTATC; reverse, ATGCT TCGGTCCACAGACTTC), *Mvh* (forward, GAAGAATTACCAGGGCA AGC; reverse, TGCTTTAATCCCATGACTCG), *Stra8* (forward, AGACC ATGGACCTCCTGACC; reverse, CAGAGAGAGTCTGCCACAGG); *Gata4* (forward, AGCAGGACTCTTGGAACAGC; reverse, CGAGCAGG AATTTGAAGAGG), *Stam2* (forward, TGATGCCTCTGTTCACTGC; reverse, CTCCAAGAAGGGTCAATGC), *Actn1* (forward, TCAGCCAGG AACAGATGAACG; reverse, AAGCGGTTGGGGTCTACAATG), *Dzip1* (forward, TCCTACAAAGCCACATCCAGCG; reverse, CCCTCATAAA CATCCCCTTGACC), *Pum2* (forward, TTAGAATCTCGGGGAATG; reverse, GTCCATCTTTTGTTGAATCATCAGG), and *Wdr7* (forward, TC CACCCTCCAGTAACATTG; reverse, AGTGCATGGCGGCTAAC).

RESULTS

Germ cell-specific inactivation of Ptbp2. Due to the early perinatal lethality of mice with global inactivation of Ptbp2 (13, 14), a Cre-lox conditional knockout approach was used to investigate the requirement and roles of Ptbp2 in postnatal male germ cell development (33). To do so, we used mice bearing the *Ptbp2*^{flox} allele developed by Li et al. (14). This allele contains *loxP* sites that allow Cre-dependent excision of genomic DNA encompassing exon 4 to generate the *Ptbp2*$^{\Delta E4}$ allele. Transcripts derived from

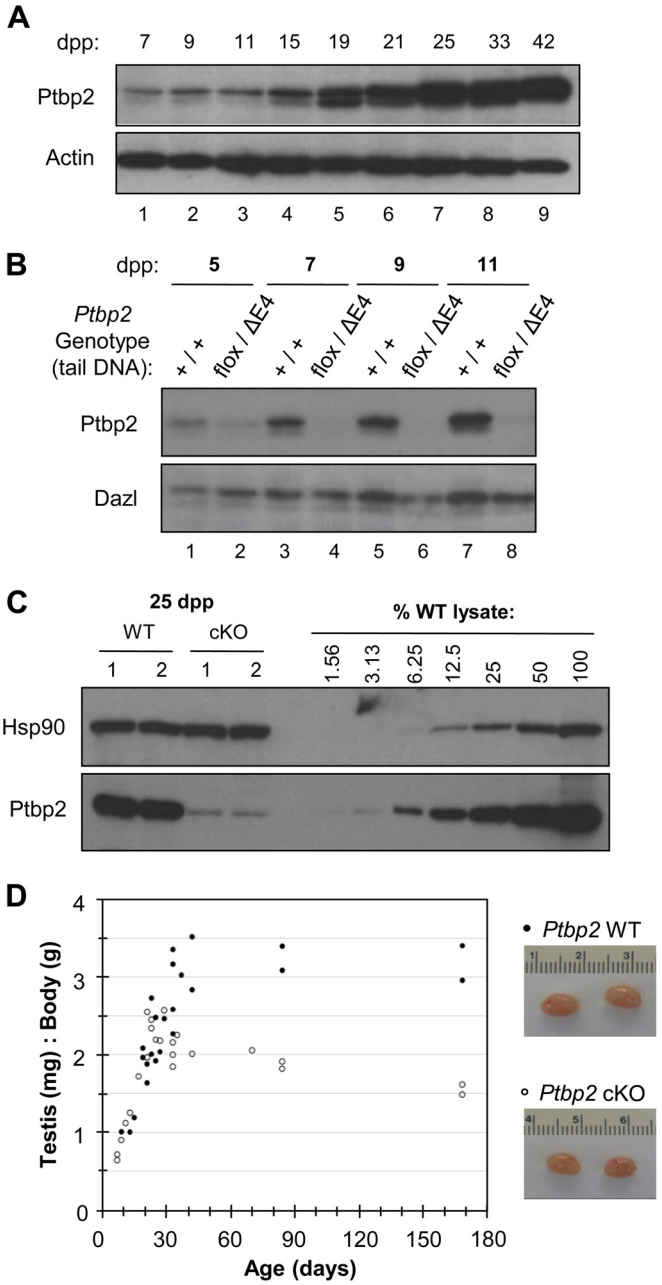

FIG 1 Conditional inactivation of *Ptbp2* expression in mouse testis. (A) Ptbp2 levels during postnatal testis development. Western blot analysis of WT testis extract prepared from testes collected on the indicated day postpartum (dpp). (B) Early postnatal decline in Ptbp2 levels in cKO testes. Analysis of Ptbp2 levels in WT and cKO testis extract, with the germ cell-specific RBP Dazl serving as a loading control. (C) A low level of Ptbp2 persists in cKO testes. Analysis of Ptbp2 levels in two WT and two cKO P25 testes, compared to a serial dilution of WT testis. Hsp90 serves as a loading control. (D) Comparison of ratios of average testis weight to whole body weight in WT and cKO mice, with photographs of 42-dpp testes displayed at right (bars in centimeters).

Ptbp2$^{\Delta E4}$ are spliced into unproductive mRNAs that contain multiple premature translation termination codons and are degraded. To recombine *Ptbp2*^{flox} to *Ptbp2*$^{\Delta E4}$ in male germ cells, we used mice bearing the *Stra8-iCre* transgene from which Cre expression begins in a subset of undifferentiated type A spermatogonia as

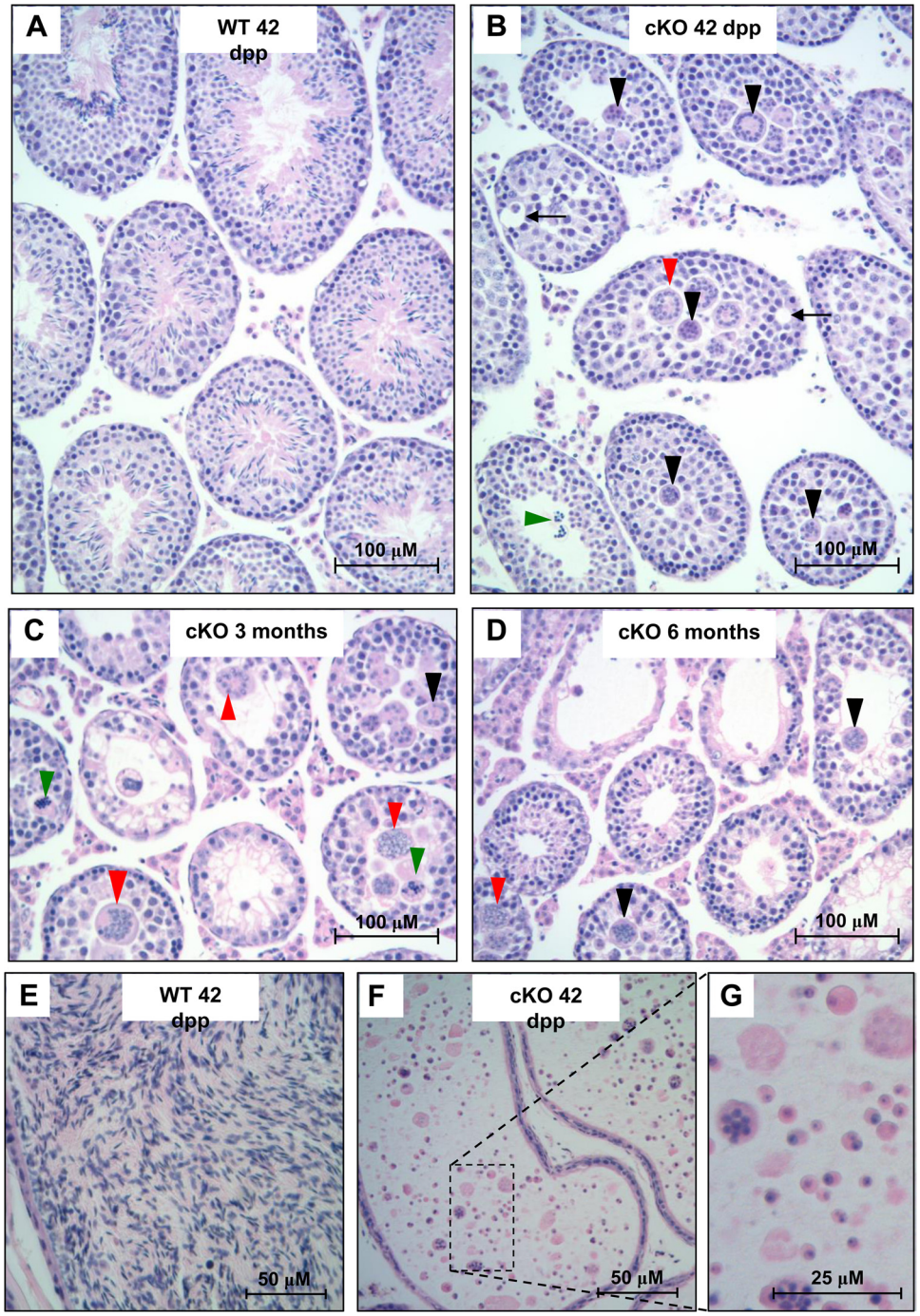

FIG 2 Spermatogenic arrest and germ cell loss in cKO testes. (A to D) Hematoxylin and eosin staining of WT testis at 42 dpp (A) and cKO testes at 42 dpp (B), 3 months (C), and 6 months (D). Black arrowheads indicate MNCs, red arrowheads indicate MNCs with chromatin condensation, green arrowheads represent MNCs with pyknotic nuclei, and arrows indicate vacuoles. (E and F) Hematoxylin and eosin staining of cauda epididymis from 24-week-old WT (E) and cKO (F) mice. (G) Higher-magnification image of the box in panel F.

early as 3 days postpartum (dpp) and ends in preleptotene spermatocytes (34, 35).

Stra8-iCre$^{+/+}$, *Ptbp2*$^{+/\Delta E4}$ males were mated with *Ptbp2*$^{+/flox}$ females to generate mice with Ptbp2-deficient testes (*Stra8-iCre*$^{+}$, *Ptbp2*$^{flox/\Delta E4}$) and wild-type controls (*Stra8-iCre*$^{+}$, *Ptbp2*$^{+/+}$), here referred to as cKO and WT, respectively. In WT testis, Ptbp2 was present at 5 and 7 dpp, when spermatogonia are the most advanced germ cell type in the testis (Fig. 1A and B). Ptbp2 levels increased dramatically at 19 dpp (Fig. 1A, lane 5), just prior to the appearance of the first-round spermatids in the testis (36). In cKO testes, Ptbp2 was present at a reduced level at 5 dpp and was barely detected thereafter (Fig. 1B, lanes 2, 4, 6, and 8). As in the brain (13, 14), Ptbp1 levels were unaffected by deletion of Ptbp2 in testes (data not shown). Additional analyses showed that Ptbp2 was re-

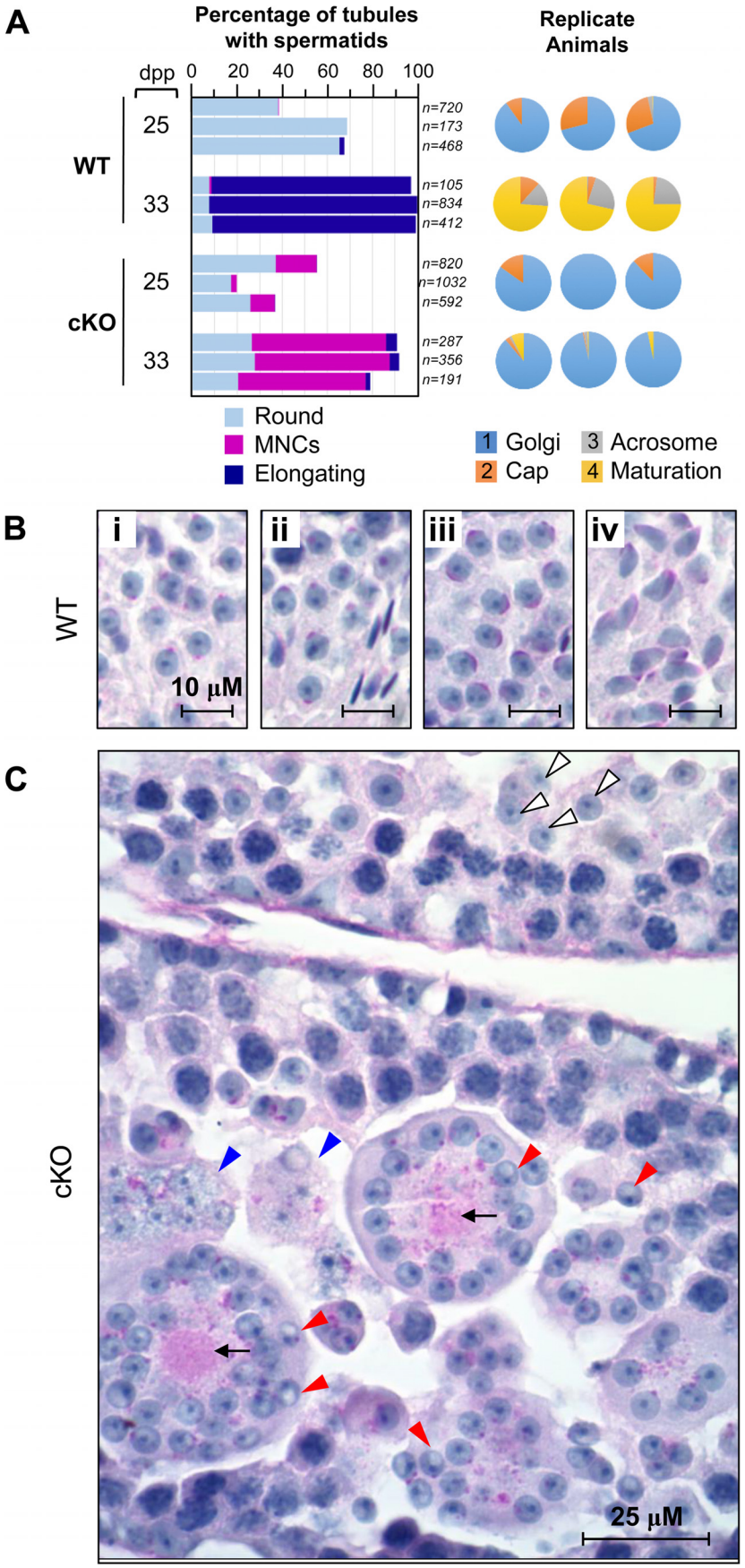
A
Percentage of tubules with spermatids
Replicate Animals
dpp
0
20
40
60
80
100
WT
25
33
cKO
25
33
n=720
n=173
n=468
n=105
n=834
n=412
n=820
n=1032
n=592
n=287
n=356
n=191
Round
MNCs
Elongating
1 Golgi
2 Cap
3 Acrosome
4 Maturation
B
WT
i
ii
iii
iv
10 μM
C
cKO
25 μM

duced to below 5% of that present in WT controls, suggesting that a small proportion of germ cells may have escaped Cre-lox-mediated ablation of Ptbp2 expression (Fig. 1C). We cannot exclude the possibility that the low level of residual Ptbp2 represents weak expression in somatic cells. Nonetheless, the *Ptbp2* cKO model described here is a powerful tool to investigate the biologic and molecular roles of Ptbp2 in an *in vivo* model system of mammalian spermatogenesis.

Ptbp2 loss results in the absence of spermatozoa. To determine how loss of Ptbp2 affects spermatogenesis, we examined testes and epididymides from WT and cKO animals over a range of prepubertal and adult ages. cKO and WT testes were comparable in size and weight until ~33 dpp, when cKO testes showed a marked reduction in the average testis weight/body weight ratio (Fig. 1D). Extensive cytological defects were also evident (Fig. 2). All stages of the seminiferous epithelial cycle were observed in testes of adult (42-dpp) WT mice (Fig. 2A) with most tubules containing elongating spermatids as expected (36). In contrast, tubules of cKO mice were smaller in diameter and lacked elongating spermatids (Fig. 2B).

The most prominent feature of Ptbp2 cKO tubules was the presence of round spermatids in the lumen, most commonly as giant multinucleated cells (MNCs) containing several spermatid nuclei (Fig. 2B to D, black arrowheads, and 3C). Formation of MNCs has been attributed to loss of germ-Sertoli cell adhesion and dissolution of the intercellular bridges that link sister germ cells (37, 38). These bridges result from incomplete cytokinesis at the end of each mitotic and meiotic division and are severed in the last steps of spermiogenesis just prior to germ cell detachment and release into the lumen (39).

After their formation, MNCs displayed apoptotic features, including progressive chromatin condensation (Fig. 2B to D and 3C, red arrowheads), cell shrinkage (Fig. 3C, blue arrowheads), and, less frequently, pyknotic nuclei (Fig. 2C and D, green arrowheads). Also evident in the cKO tubules were large vacuoles (Fig. 2B, arrows). With increasing age, cKO testes displayed progressive germ cell loss and seminiferous tubule atrophy, with some tubules showing nearly complete germ cell loss and extensive vacuolization (Fig. 2C and D). Accordingly, the epididymides of cKO mice were devoid of spermatozoa and contained immature spermatids and MNCs instead (Fig. 2E to G). Therefore, Cre-mediated inactivation of *Ptbp2* resulted in the absence of spermatozoa due to a block in spermatid differentiation.

Ptbp2-null spermatids become multinucleate during the first steps of differentiation. Histological examination of prepubertal testes showed that premature detachment of spermatids in the form of MNCs occurred during the first wave of spermatogenesis in cKO mice. At 25 dpp, the majority of WT spermatids had not yet progressed into the elongating steps of differentiation, with multinucleated cells rarely observed (Fig. 3A). In contrast, MNCs were readily detected at 25 dpp in cKO testes and present in the majority of spermatid-containing tubules at 33 dpp (Fig. 3A).

Spermatid differentiation can be subdivided into 16 steps. To more specifically determine the step(s) of differentiation when spermatid arrest occurred, tissue sections were stained with periodic acid-Schiff (PAS) stain to detect glycoproteins present in the acrosome (40). The acrosome is a Golgi complex-derived structure required for proper formation of the spermatozoan head region and for oocyte penetration (41). An early step in acrosome formation is the attachment of the acrosomal granule to the spermatid nucleus, where it then flattens (at step 4) and extends over the nuclear surface of round and elongating spermatids. As expected, spermatids in all steps of differentiation were readily identified in WT testes at 33 dpp (Fig. 3B, i to iv), with the majority being elongating spermatids in the final (maturation) phase of acrosome biogenesis (Fig. 3A, pie charts at right). In contrast, the majority of PAS-positive structures associated with cKO spermatid nuclei were punctate (Fig. 3C) and flattening of the acrosome to the spermatid nuclear membrane was rarely observed. Importantly, cKO round spermatids in tubules that did not contain MNCs generally lacked PAS-positive material, indicating that they were newly generated (Fig. 3C, white arrowheads). Together, these observations indicate that cKO germ cell arrest and MNC formation occurred during the Golgi phase of acrosome biogenesis (steps 1 to 3 of spermatid differentiation). Interestingly, PAS staining also revealed an accumulation of glycoproteins in the cytoplasm of MNCs, suggesting a potential defect in the secretion of glycosylated proteins in the absence of Ptbp2 (Fig. 3C, arrows).

Multiparameter, dual fluorescence separation of germ and somatic cells. With the goal of obtaining a quantitative overview of spermatogenesis in cKO testes, we sought to establish a dual fluorescence flow cytometry procedure to discriminate, quantify, and collect germ cells in each of the major stages of spermatogenesis. This strategy builds upon a well-established flow cytometry procedure that uses the DNA binding dye Hoechst 33342 (Ho), a UV-excitable dye with a primarily blue fluorescence emission spectrum. As the concentration of DNA-bound Ho increases, a spectral shift toward increased red fluorescence emission occurs (42–44). The dual (blue/red) emission of Ho has been exploited to differentially stain cells from mouse seminiferous tubules based on dye efflux, DNA ploidy, and chromatin structure/accessibility (26–28, 45). While it is a powerful quantitative and preparative tool, a limitation of this approach is that diploid germ cells and somatic cells appear as a single extended cluster of cells with overlapping blue and red fluorescence emission values (*y* and *x* axes, respectively, in Fig. 4C and 5D). The inability to resolve these cells hinders the discrimination and quantification of somatic cells and germ cells in different stages of spermatogenesis.

FIG 3 Spermatid arrest and multinucleate cell formation occur in the early steps of differentiation. (A) Quantification of spermatids in seminiferous tubules from 12 different animals collected on the indicated days (three animals per time point). The graph at left indicates the percentages of tubule cross sections containing round, multinucleate, or elongating spermatids. Pie charts (right) indicate proportions of spermatid-containing tubules with spermatids in the four stages of acrosome biogenesis: (1) Golgi stage, (2) cap, (3) acrosome, and (4) maturation. (B) Detection of spermatids in different stages of acrosome development in 33-dpp WT testis by PAS and hematoxylin staining. (i) Proacrosomal granules; (ii) acrosomal granules that have attached to spermatid nuclei; (iii) acrosomal granules that have attached to and flattened against spermatid nuclei; (iv) elongating spermatids with acrosomes extending over the nuclei. (C) PASH staining of 33-dpp cKO testis shows punctate PAS-positive acrosomal granules associated with spermatid nuclei and accumulation of PAS-positive material in the cytoplasm of multinucleated cells. Also evident are spermatid nuclei with crescent-shaped clearings indicative of chromatin condensation (red arrowheads) and MNCs that have undergone cell shrinkage and contain nuclei with more advanced condensation (blue arrowheads). Early-stage spermatids that are PAS negative and have not yet become MNCs are indicated with white arrowheads, while PAS-positive material accumulating in the center of MNCs is indicated with arrows.

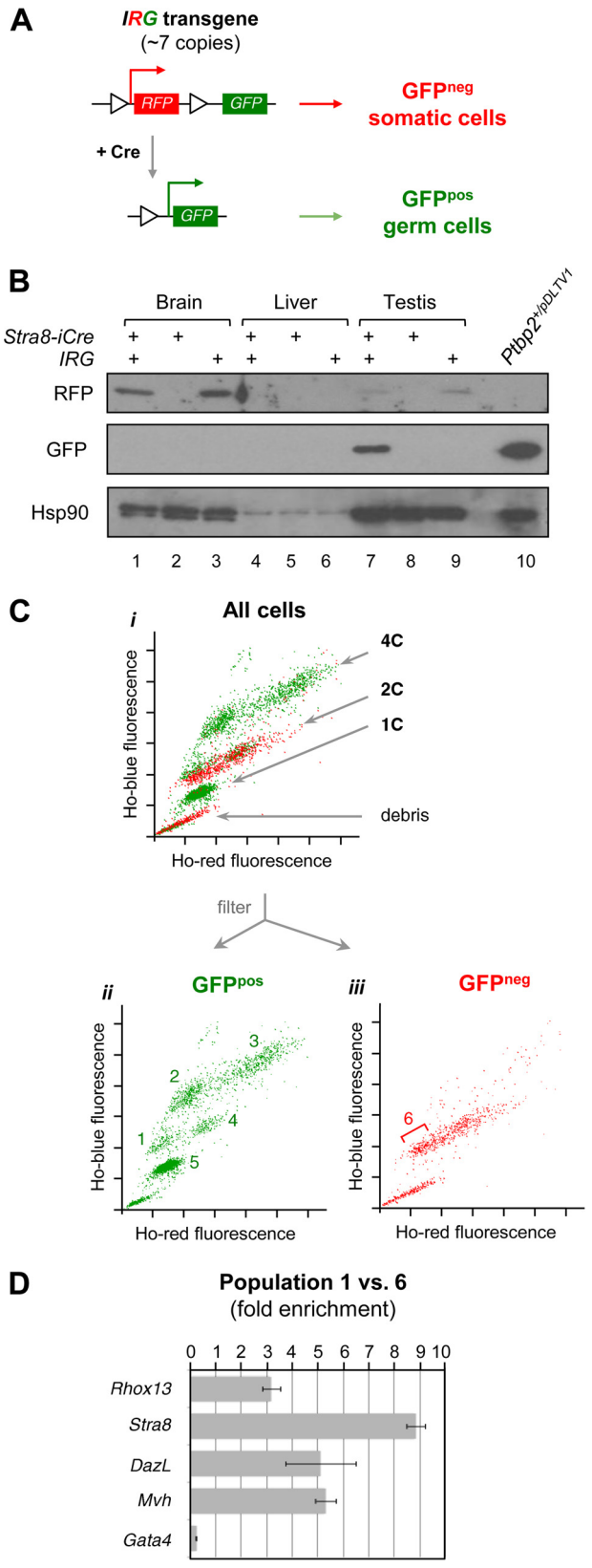

FIG 4 Separation of Ho-stained GFP^{pos} germ cells by flow cytometry. (A) Schematic of the *IRG* transgene before and after Cre-lox recombination. (B) Western blot analysis of *IRG* transgene expression in brain, liver, and testes from mice containing the *Stra8-iCre* and/or *IRG* transgene. As a positive control for GFP expression, brain lysate from a *Ptbp2*$^{+/pDLTV1}$ mouse was included. The *Ptbp2*^{pDLTV1} allele was generated by homologous recombination to replace essential coding sequence from exon 1 with coding sequence for enhanced GFP (13). Consistent with the work of De Gasperi et al. (46), RFP expression was detected in brain and absent in liver. Importantly, RFP expression was confirmed in testis of *IRG*$^{+}$ (lane 9) and *Stra8-iCre*$^{+}$;*IRG*$^{+}$ (lane 7) mice, while GFP expression was detected in testes of *Stra8-iCre*$^{+}$;*IRG*$^{+}$ mice (lane 7). Hsp90 serves as a loading control. (C) Distribution of Hoechst 33342-stained cells from *IRG*$^{+}$ WT testis. 1C, 2C, and 4C cells segregate as three distinct bands with increasing blue and red fluorescence. Panels correspond to all cells (i), GFP^{pos} cells (ii), and GFP^{neg} cells (iii). GFP^{pos} cells cluster into 5 subpopulations, previously demonstrated to correspond to (1) spermatogonia, (2) early-prophase spermatocytes, (3) late-prophase I spermatocytes, (4) secondary spermatocytes, and (5) spermatids. Population 6 (iii) corresponds to diploid GFP^{neg} cells with blue and red fluorescence values that overlap those of GFP^{pos} population 1. (D) Quantitative RT-PCR analysis of germ cell transcripts (*Rhox13*, *Stra8*, *Dazl*, and *Mvh* relative to *Actb* transcripts) and the somatic cell transcript *Gata4* (relative to *Actb* transcripts) in GFP^{pos} population 1 cells versus GFP^{neg} population 6 cells.

To overcome this obstacle, we performed Ho staining and flow cytometry on seminiferous tubules from dual fluorescence transgenic animals that have green fluorescent protein (GFP) expression in germ cells and red fluorescent protein (RFP) expression in somatic cells. To do so, we generated animals that contained the *Stra8-iCre* transgene (described above) and the *IRG* transgene (46), an RFP-to-GFP dual fluorescence reporter that contains RFP cDNA flanked by *loxP* sites and followed by coding sequence for GFP (Fig. 4A). Cre-dependent recombination serves as a switch to allow GFP expression. We first confirmed that the *IRG* transgene was expressed in mouse testis by Western blot analysis of RFP and GFP expression in single- and double-transgenic mice bearing the *IRG* and *Stra8-iCre* transgenes (Fig. 4B).

As previously demonstrated (26, 27), total Ho-stained cells prepared from adult testes showed characteristic bands of 1C, 2C, and 4C cells with increasing fluorescence emission values (Fig. 4C, i), independent of the presence of the IRG transgene (data not shown). After gating cells for GFP expression, pronounced differences in the GFP-negative (GFP^{neg}) and GFP-positive (GFP^{pos}) cell populations were observed. The GFP^{neg} population consisted primarily of a single broad cluster of diploid cells (Fig. 4C, iii). In contrast, GFP^{pos} cells consisted of 5 distinct cell populations, numbered to reflect germ cells in advanced steps in spermatogenesis. Importantly, GFP gating partitioned diploid GFP^{pos} cells into two distinct clusters (populations labeled 1 and 4 in Fig. 4C, ii), corresponding to spermatogonia and secondary spermatocytes, respectively. The identities of these cells, as well as the two major 4C populations (labeled 2 and 3, corresponding to early- and late-prophase-I spermatocytes, respectively) and the single cluster of 1C cells (population 5, spermatids), have been previously established using immunohistochemistry, expression profiling, and genetic models with stage-specific germ cell arrest (26–28, 47).

To further assess the utility of GFP gating to resolve diploid germ cells and somatic cells, quantitative RT-PCR analysis was used to assess the levels of germ cell and somatic cell transcripts in GFP^{pos} and GFP^{neg} cells with overlapping blue and red fluorescence emissions (populations 1 and 6, respectively). Relative to beta-actin transcripts (*Actb*), germ cell transcripts (*Rhox13*, *Dazl*, *Mvh*, and *Stra8*) were significantly enriched in GFP^{pos} cells (~3- to 9-fold [Fig. 4D]) compared to GFP^{neg} cells. Conversely, *Gata4* transcripts were underrepresented, consistent with *Gata4* expression being restricted to somatic Sertoli cells. These observations are consistent with the GFP^{neg} dip-

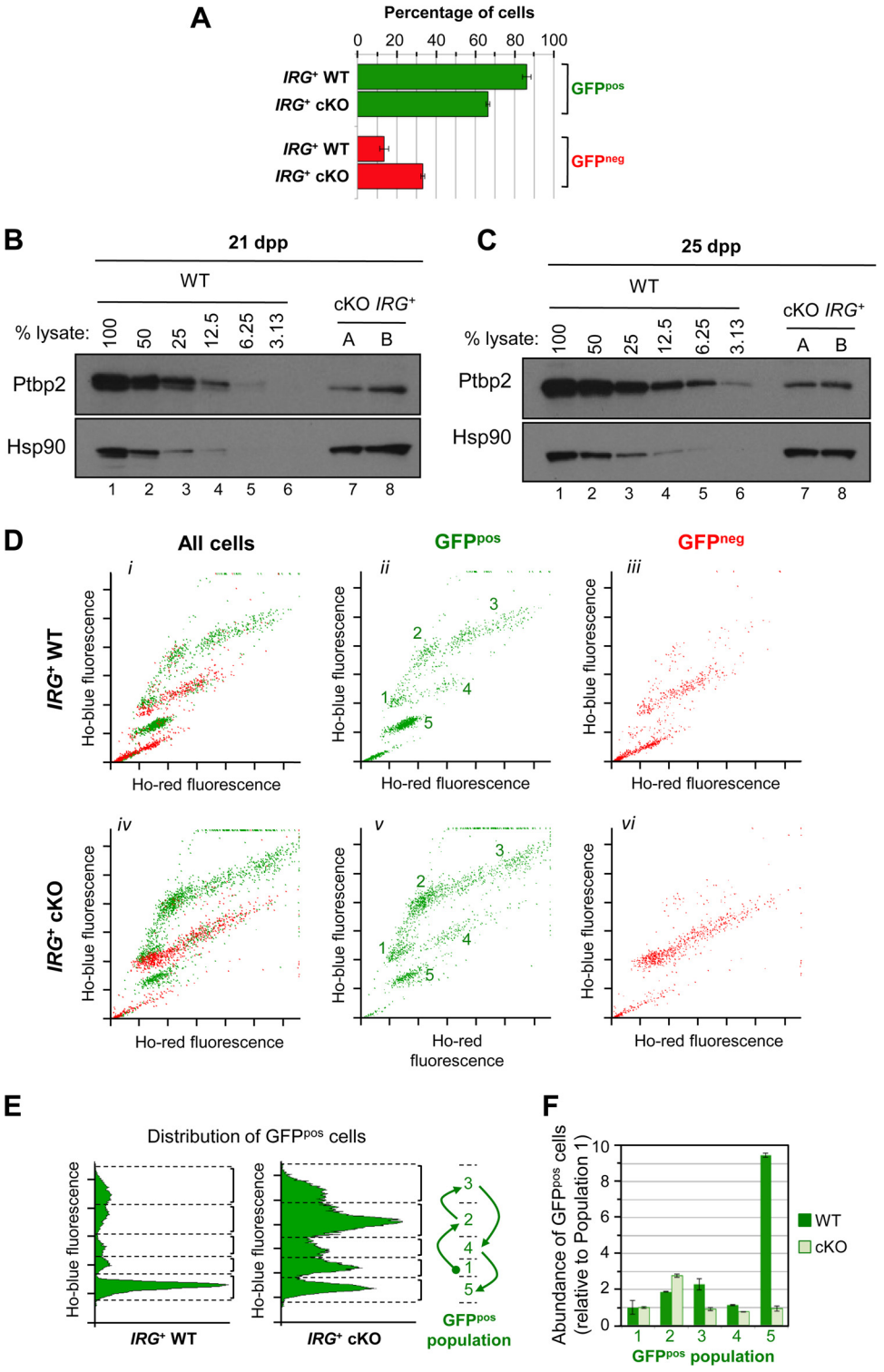

FIG 5 Flow cytometry of Ho-stained cells from *IRG*$^+$ WT and cKO testes. (A) Average percentages of GFP^{pos} and GFP^{neg} cells in testes from two WT and two cKO 9-week-old mice. (B and C) Western blot analyses of Ptbp2 levels in two *IRG*$^+$ cKO animals at 21 dpp (B, lanes 7 and 8) and two *IRG*$^+$ cKO animals at 25 dpp (C, lanes 7 and 8). Lanes 1 to 6 represent serial dilutions of WT testis lysate collected from 21- and 25-dpp mice (B and C, respectively). (D) Distribution of all cells (5,000 events) (i and iv), GFP^{pos} cells (ii and v), and GFP^{neg} cells (iii and vi) from *IRG*$^+$ WT (i to iii) and *IRG*$^+$ cKO (iv to vi) testes. (E) Distribution of GFP^{pos} cells in different stages of spermatogenesis based on blue fluorescence values from data presented in panel D. (F) Quantification of WT and cKO germ cells in different GFP^{pos} populations, relative to population 1 (mitotic) cells.

loid cells consisting primarily of somatic cells and any spermatogonia that have not yet undergone a switch from RFP to GFP expression. In addition, the data indicate that the majority of spermatogonia are GFP labeled in the *Stra8-iCre*$^{+}$, *IRG*$^{+}$ testis and that Ho staining in combination with GFP gating provides a means to distinguish and separate them from somatic cells with similar Ho emission values. Importantly, GFP^{pos} germ cells in each of the major stages of development were readily observed, indicating that GFP derived from the *IRG* transgene is present throughout spermatogenesis. Furthermore, the absence of 1C and 4C GFP^{neg} cells indicates efficient recombination of the *IRG* transgene in *Stra8-iCre*$^{+}$ testes. Collectively, these observations indicate that Ho staining and flow cytometry of GFP^{pos} cells from *IRG*$^{+}$, *Stra8-iCre*$^{+}$ seminiferous tubules are an effective strategy to distinguish germ and somatic cells in the testis and to quantify and collect germ cells in different stages of spermatogenesis.

Quantitative analysis of germ cell populations in Ptbp2-deficient testis. To use dual fluorescence flow cytometry to analyze germ cell populations in Ptbp2-deficient testes, the *IRG* transgene was bred into the *Ptbp2*$^{+/flox}$ females used to generate WT and cKO animals. Consistent with the germ cell loss observed histologically, fewer GFP^{pos} cells were detected in adult *IRG*$^{+}$ cKO testis than in *IRG*$^{+}$ WT controls (66% versus 86% of total, respectively) (Fig. 5A).

Consistent with incomplete Cre-mediated recombination when multiple floxed alleles are present (48), the level of residual Ptbp2 was elevated (~10% compared to WT) in cKO *IRG*$^{+}$ testes compared to cKO testes lacking the *IRG* transgene (Fig. 5B and C). In contrast, the percentage of meiotic GFP^{neg} cells did not increase in cKO, as would be expected if the efficiency of GFP labeling (RFP-to-GFP recombination) was reduced in the presence of the *Ptbp2*^{flox} allele. A possible explanation for this difference is that the *IRG* locus contains an estimated 7 to 10 copies of the *IRG* cassette (46). Thus, even under conditions of reduced overall recombination activity when multiple floxed alleles are present (48), the high copy number of the *IRG* cassette permits efficient labeling of germ cells with GFP.

In addition to an overall reduction in germ cells in Ptbp2-null testis, the distributions of these cells in different stages of spermatogenesis were markedly different (Fig. 5D to F). The most abundant germ cell type present in WT adult testes was spermatids (GFP^{pos} population 5), as expected (36). In contrast, spermatids were significantly reduced in *IRG*$^{+}$ cKO testes, consistent with their premature detachment and MNC formation. Differences in meiotic germ cells were also identified by flow cytometry of *IRG*$^{+}$ cKO testes, as indicated by a reduction in the number of late-stage spermatocytes (population 3) that was accompanied by an accumulation of early-stage spermatocytes (population 2) (Fig. 5E and F).

To assess whether apoptosis contributes to the reduction of spermatocytes in the absence of Ptbp2, TUNEL assays were used to label apoptotic cells with fragmented DNA. Seminiferous tubules with TUNEL-positive cells were more frequently observed in 33-dpp cKO testes than in WT controls (Fig. 6A). Unlike TUNEL-positive cells in WT testis, which are mostly spermatogonia adjacent to the basal membrane, the morphology and position of cKO TUNEL-positive cells indicate that they are predominantly spermatocytes (Fig. 6A and B). Notably, nuclei within MNCs were TUNEL negative (Fig. 6C, arrows). Together, these observations suggest that increased spermatocyte apoptosis contributes to the reduction in late-prophase-I spermatocytes (GFP^{pos} population 3) observed by dual fluorescence flow cytometry of *IRG*$^{+}$ cKO testes.

Collectively, flow cytometry analysis of GFP^{pos} cKO germ cells in combination with histological analyses demonstrated that Ptbp2 was essential for spermatogenesis, with cKO germ cells arresting at two different stages. A partial block to spermatogenesis occurred in a subset of germ cells in meiosis I and was manifested by an accumulation of spermatocytes in early prophase and increased spermatocyte apoptosis. The surviving Ptbp2-deficient spermatocytes completed meiosis only to yield spermatids that arrested at an early stage of differentiation and were prematurely released into the tubule lumen, most frequently as MNCs.

Ptbp2 is required for proper splicing of germ cell mRNAs. The failure of Ptbp2-null germ cells to complete spermatogenesis suggests an essential role for this RBP in posttranscriptional regulation of germ cell RNAs. Given the importance of Ptbp2 as a regulator of AS in the brain (13, 14), we first explored the possibility that Ptbp2 is required for proper expression of AS RNAs in the testis. To do so, we used RT-PCR to measure the relative levels of AS RNA isoforms in WT and cKO testes at 21 and 25 dpp. For this analysis, we examined a subset of alternative exons identified by splicing microarray analysis and confirmed by RT-PCR whose splicing regulation is dependent on Ptbp2 in brain. Additionally, we focused on candidates for which HITS-CLIP (high-throughput sequencing of RNA isolated by cross-linking immunoprecipitation) analysis in brain provided evidence of direct Ptbp2 RNA binding to evolutionarily conserved sequences flanking the regulated exons (13). In nearly all cases, exons that were repressed in a Ptbp2-dependent manner in brain were also dependent on Ptbp2 for proper splicing regulation in 21- and 25-dpp testes (Fig. 7A and B, respectively). A notable exception was the regulation of *Actn1* RNAs generated by AS of the nonmuscle (NM) and smooth muscle (SM) exons (Fig. 7A, iii). Whereas Ptbp2 loss resulted in a robust switch in the expression of *Actn1* AS isoforms in brain (Fig. 7A, iii, lanes 5 and 6), no change was observed in WT and cKO testes. Importantly, the relative levels of the exon-spliced and skipped AS variants were highly reproducible between biological replicates, including WT and cKO testes with or without the *IRG* transgene (Fig. 7A). These observations indicate that Ptbp2 is necessary for proper control of AS RNA expression during the first wave of spermatogenesis and is required for regulation of overlapping but distinct sets of AS exons in brain and testis.

A role for Ptbp2 in the stabilization of germ cell transcripts that undergo stage-specific translation has also been suggested but not directly examined in testes. Based on results from cell culture and *in vitro* assays with cell extract and synthetic RNA, Ptbp2 has been proposed to have a role in the stabilization of *Pgk2* transcripts (24). *Pgk2* mRNA is first detected in spermatocytes and present at elevated levels in spermatids, while Pgk2 protein is restricted to the latter (49). To investigate whether Ptbp2 loss affects *Pgk2* mRNA abundance *in vivo*, we used real-time RT-PCR to examine *Pgk2* transcript levels in WT and cKO meiotic cells collected by dual fluorescence flow cytometry (Fig. 7C). Relative to actin transcripts (*Actb*), no significant difference in *Pgk2* RNA abundance was apparent in GFP^{pos} spermatocytes, where stabilization of *Pgk2* mRNAs by Ptbp2 has been suggested to occur. Thus, while we cannot rule out a splicing-independent role for Ptbp2 in posttranscriptional regulation of germ cell

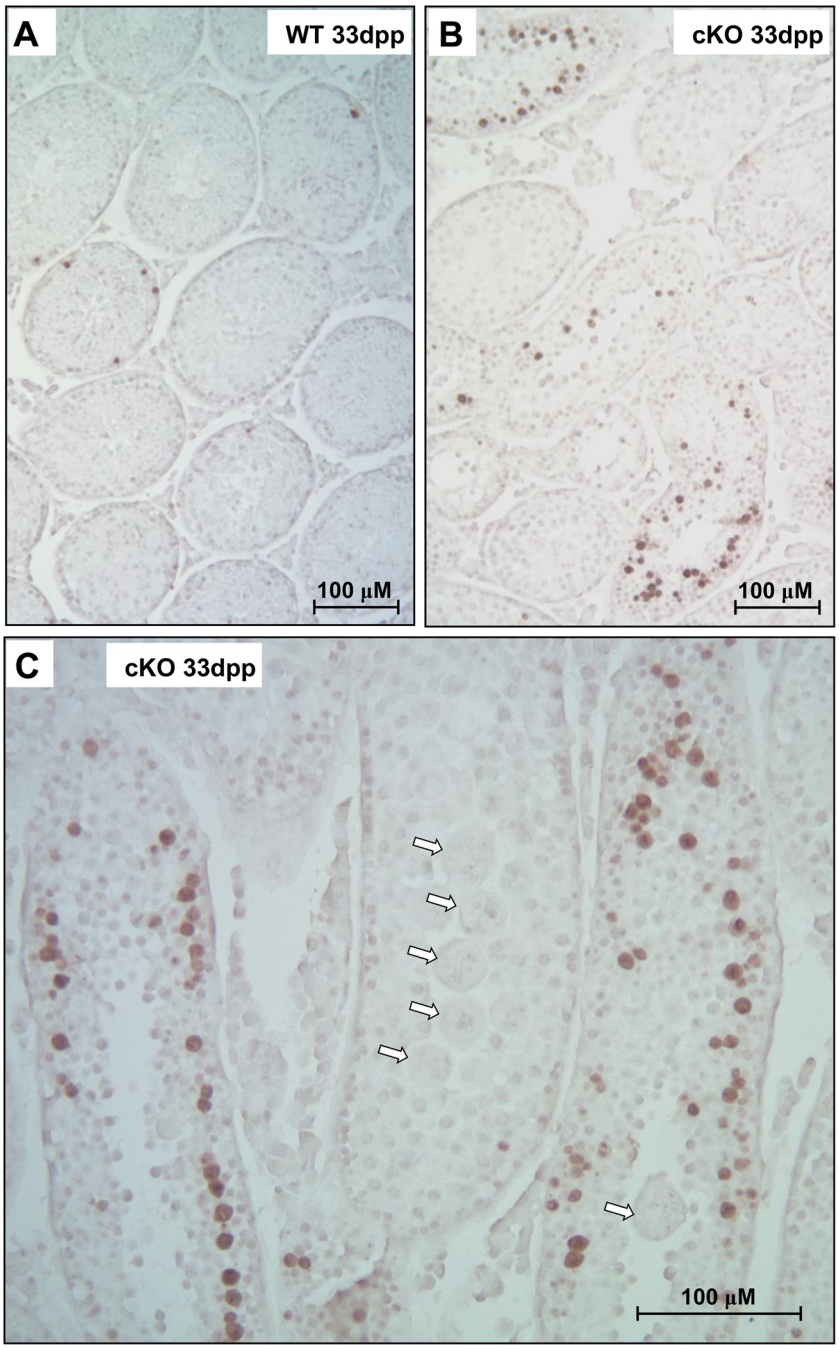

FIG 6 Increased apoptosis of spermatocytes in cKO testes. TUNEL staining of WT (A) and cKO (B and C) testes at 33 dpp. Arrows denote TUNEL-negative MNCs.

RNAs, we conclude that Ptbp2 is not required for stabilization of *Pgk2* mRNA in spermatocytes.

DISCUSSION

RBPs are increasingly recognized as critical posttranscriptional regulators of gene expression, having central roles in tissue development, homeostasis, and disease (2, 50). Tissue-specific AS is a prominent posttranscriptional regulatory process that remodels protein-protein interaction networks and specializes cell functions (51, 52). Accordingly, AS is highly regulated to ensure that the correct complement of AS RNA and protein variants is expressed in the correct cell type at the correct time. In the nervous system, the tissue-restricted RBP Ptbp2 has important roles in developmental stage-specific control of AS RNAs. In this work, we demonstrate that Ptbp2 is an essential spermatogenic factor, whose function(s) cannot be compensated for by other RBPs present in germ cells. In addition, we show that Ptbp2 is required for correct expression of AS mRNA variants in the testis.

Multiple spermatogenic defects were observed in Ptbp2 cKO testes using both traditional histological tools and the dual fluo-

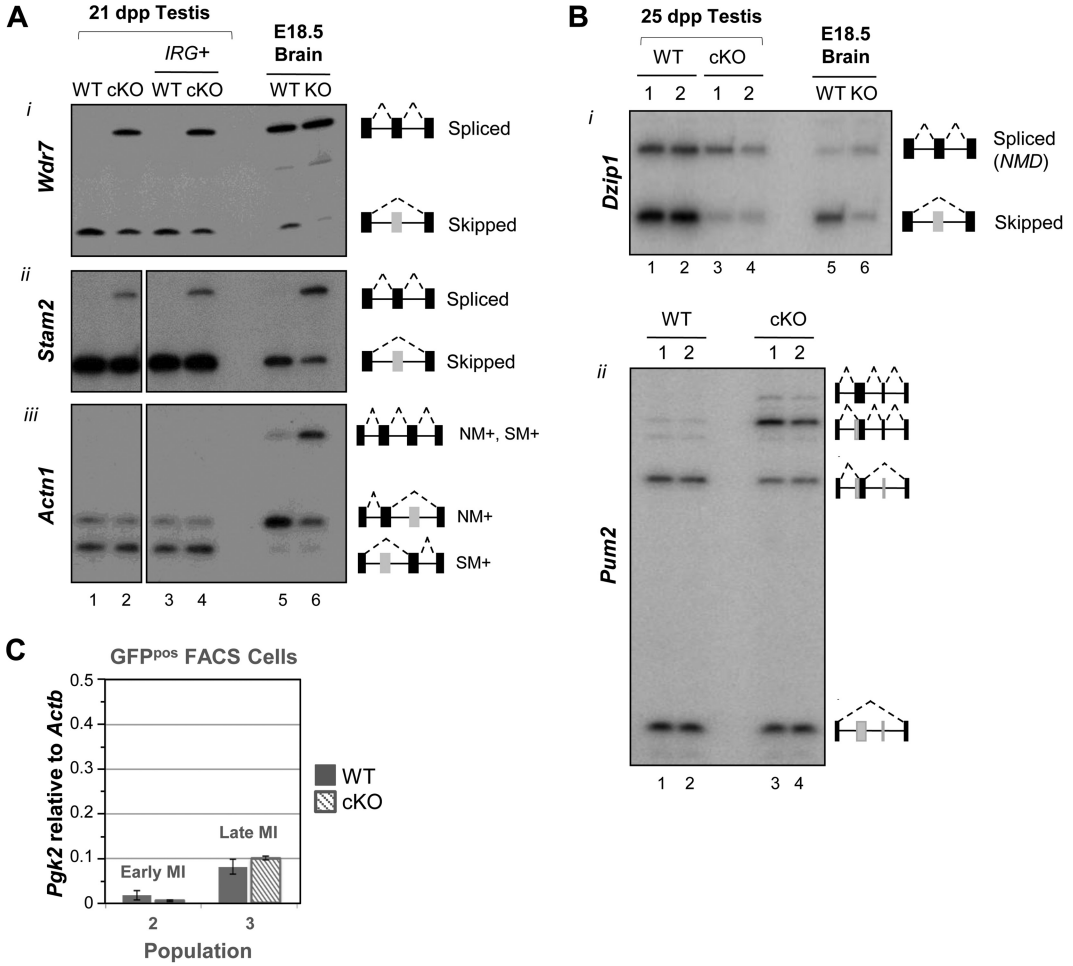

FIG 7 Ptbp2 is required for AS regulation in the testis. (A) RT-PCR analysis of AS RNAs from the *Wdr7* (i), *Stam2* (ii), and *Actn1* (iii) genes in testes from 21-dpp WT and cKO mice without (lanes 1 and 2) and with (lanes 3 and 4) the *IRG* transgene. Lanes 5 and 6 correspond to embryonic brain from embryonic day 18.5 (E18.5) WT and Ptbp2-deficient mice generated by timed matings of $Ptbp2^{+/pDLTV1}$ animals (13). (B) RT-PCR analysis of AS RNA from the *Dzip1* (i) and *Pum2* (ii) genes in testes from two biological replicates of 25-dpp WT and cKO testes (lanes 1 and 2 and lanes 3 and 4, respectively), with embryonic brain included in the top panel (*Dzip1*), as described above. (C) Quantitative RT-PCR analysis of *Pgk2* RNA levels (relative to *Actb*) in early- and late-prophase-I spermatocytes (GFP^{pos} populations 2 and 3, respectively) purified by flow cytometry of Ho-stained IRG^{+} WT and IRG^{+} cKO testes. FACS, fluorescence-activated cell sorting; MI, meiosis I.

rescence flow cytometry approach described here. These include increased vacuolization, increased apoptosis of spermatocytes, premature detachment of spermatids, MNC formation, and the accumulation of glycosylated proteins in the cytoplasm of MNCs. Notably, spermatogenic defects occurred largely in spermatocytes and spermatids that normally display increases in Ptbp2 levels. These observations suggest that regulation of AS RNA isoforms by Ptbp2 may have important roles in transcriptome remodeling events necessary for germ cell progression through the meiotic and postmeiotic stages of spermatogenesis.

Interestingly, several of the defects observed in Ptbp2 cKO testes resemble phenotypic features of mouse knockout models lacking proteins involved in germ-Sertoli cell adhesion and signal transduction. For example, increased germ cell apoptosis and MNC formation occur in mice lacking the serine-threonine kinase Akt1, which participates in a prosurvival signaling cascade in response to trophic factors (53). Similar defects also occur in mouse testes lacking the fibronectin domain-containing protein FNDC3A (originally described as the symplastic spermatid "sys" mutation [37, 54]), the glycosylated cell adhesion molecule Cadm1 (55, 56), the multifunctional glycoprotein Basigin (57), and the glycosyltransferase Mgat1 (58). Strikingly, loss of Sertoli cell-restricted proteins (Cib1, Inpp5b, and Gata4) also results in apoptosis of germ cells and MNC formation (59–61), further highlighting the importance of germ-Sertoli cell interaction. Notably, cKO MNCs displayed apoptotic features, including chromatin condensation and cell shrinkage, but were TUNEL negative, suggesting that apoptosis of spermatocytes and spermatids in cKO testes may occur via distinct mechanisms. Similarly, MNCs that form in Cib1-null mice are also TUNEL negative (59). How Ptbp2 loss affects posttranscriptional regulation of the abovementioned genes or the large number of genes with related functions will require a more comprehensive analysis of the cKO transcriptome in different spermatogenic cell types.

Hoechst staining and flow cytometry are a powerful method for the study of spermatogenesis (26–31, 47). While this approach allows the discrimination of seminiferous tubule cells based on DNA content (1C, 2C, and 4C), chromatin structure,

and dye efflux, the cellular heterogeneity of the 2C population (consisting of spermatogonia, secondary spermatocytes, and somatic cells with similar fluorescence emission properties) compromises the quantification and collection of germ cells in different stages of spermatogenesis. Here, we demonstrated that GFP labeling of germ cells in animals containing the *Stra8-iCre* and *IRG* transgenes is an effective strategy to distinguish germ cells from somatic cells. Importantly, GFP^{pos} cells in each of the major stages of spermatogenesis can be readily identified. Moreover, the high copy number of the *IRG* transgene may allow efficient GFP labeling of germ cells even under conditions of reduced Cre-mediated recombination due to weak Cre expression or the presence of competing loxP sites. While the dual fluorescence flow cytometry approach improves the discrimination and quantification of germ and somatic cells, the suitability of the collected GFP^{pos} cells for different downstream applications must be empirically determined.

In summary, the phenotypic features revealed by histologic and flow cytometric analyses of cKO testes in combination with RT-PCR of AS RNAs indicate that posttranscriptional regulation by Ptbp2 may have an important role in modulating the expression of genes necessary for proper germ cell contact and communication with Sertoli cells. The identification of these genes and insights into the molecular basis for the cKO phenotype remain to be elucidated. Strikingly, not all candidates examined were sensitive to Ptbp2 deletion in both brain and testis. This observation indicates that Ptbp2 participates in tissue-specific AS regulation of overlapping but distinct sets of RNA targets to specialize neuronal and germ cell functions. Finally, although the functional importance of the high levels of AS in testes remains to be determined, this work suggests that proper regulation of AS by Ptbp2 has a critical role in establishing the correct repertoire of RNA and protein variants necessary for cell progression through the spermatogenic pathway.

ACKNOWLEDGMENTS

We are grateful to the following individuals for their contributions to this work: Douglas Black (UCLA) for providing mice with the *Ptbp2*^{flox} allele; Nancy Edgehouse and Jenifer Mikulan at the CWRU Histology Core for tissue processing and embedding; Adam Kresak at the CWRU Tissue Resources Core for assistance with photomicroscopy; Robert Darnell for providing anti-Ptbp2 antibody; and Christopher Geyer, Timothy Nilsen, and Jo Ann Wise for comments on the manuscript.

This work was supported by NIH grant GM107331 to D.D.L.

REFERENCES

1. **Fu XD, Ares MJ.** 2014. Context-dependent control of alternative splicing by RNA-binding proteins. Nat Rev Genet **15:**689–701. http://dx.doi.org/10.1038/nrg3778.
2. **Kalsotra A, Cooper TA.** 2011. Functional consequences of developmentally regulated alternative splicing. Nat Rev Genet **12:**715–729. http://dx.doi.org/10.1038/nrg3052.
3. **Spellman R, Smith CW.** 2006. Novel modes of splicing repression by PTB. Trends Biochem Sci **31:**73–76. http://dx.doi.org/10.1016/j.tibs.2005.12.003.
4. **Keppetipola N, Sharma S, Li Q, Black DL.** 2012. Neuronal regulation of pre-mRNA splicing by polypyrimidine tract binding proteins, PTBP1 and PTBP2. Crit Rev Biochem Mol Biol **47:**360–378. http://dx.doi.org/10.3109/10409238.2012.691456.
5. **Jangi M, Sharp PA.** 2014. Building robust transcriptomes with master splicing factors. Cell **159:**487–498. http://dx.doi.org/10.1016/j.cell.2014.09.054.
6. **Lillevali K, Kulla A, Ord T.** 2001. Comparative expression analysis of the genes encoding polypyrimidine tract binding protein (PTB) and its neural homologue (brPTB) in prenatal and postnatal mouse brain. Mech Dev **101:**217–220. http://dx.doi.org/10.1016/S0925-4773(00)00566-9.
7. **Polydorides AD, Okano HJ, Yang YY, Stefani G, Darnell RB.** 2000. A brain-enriched polypyrimidine tract-binding protein antagonizes the ability of Nova to regulate neuron-specific alternative splicing. Proc Natl Acad Sci U S A **97:**6350–6635. http://dx.doi.org/10.1073/pnas.110128397.
8. **Markovtsov V, Nikolic JM, Goldman JA, Turck CW, Chou MY, Black DL.** 2000. Cooperative assembly of an hnRNP complex induced by a tissue-specific homolog of polypyrimidine tract binding protein. Mol Cell Biol **20:**7463–7479. http://dx.doi.org/10.1128/MCB.20.20.7463-7479.2000.
9. **Boutz PL, Stoilov P, Li Q, Lin CH, Chawla G, Ostrow K, Shiue L, Ares MJ, Black DL.** 2007. A post-transcriptional regulatory switch in polypyrimidine tract-binding proteins reprograms alternative splicing in developing neurons. Genes Dev **21:**1636–1652. http://dx.doi.org/10.1101/gad.1558107.
10. **Makeyev EV, Zhang J, Carrasco MA, Maniatis T.** 2007. The microRNA miR-124 promotes neuronal differentiation by triggering brain-specific alternative pre-mRNA splicing. Mol Cell **27:**435–448. http://dx.doi.org/10.1016/j.molcel.2007.07.015.
11. **Spellman R, Llorian M, Smith CW.** 2007. Crossregulation and functional redundancy between the splicing regulator PTB and its paralogs nPTB and ROD1. Mol Cell **27:**420–434. http://dx.doi.org/10.1016/j.molcel.2007.06.016.
12. **Hamid FM, Makeyev EV.** 2014. Regulation of mRNA abundance by polypyrimidine tract-binding protein-controlled alternate 5′ splice site choice. PLoS Genet **10:**e1004771. http://dx.doi.org/10.1371/journal.pgen.1004771.
13. **Licatalosi DD, Yano M, Fak JJ, Mele A, Grabinski SE, Zhang C, Darnell RB.** 2012. Ptbp2 represses adult-specific splicing to regulate the generation of neuronal precursors in the embryonic brain. Genes Dev **26:**1626–1642. http://dx.doi.org/10.1101/gad.191338.112.
14. **Li Q, Zheng S, Han A, Lin CH, Stoilov P, Fu XD, Black DL.** 2014. The splicing regulator PTBP2 controls a program of embryonic splicing required for neuronal maturation. eLife **3:**e01201. http://dx.doi.org/10.7554/eLife.01201.
15. **Yang QE, Oatley JM.** 2014. Spermatogonial stem cell functions in physiological and pathological conditions. Curr Top Dev Biol **107:**235–267. http://dx.doi.org/10.1016/B978-0-12-416022-4.00009-3.
16. **Oakberg EF.** 1956. A description of spermiogenesis in the mouse and its use in analysis of the cycle of the seminiferous epithelium and germ cell renewal. Am J Anat **99:**391–413. http://dx.doi.org/10.1002/aja.1000990303.
17. **Fawcett DW.** 1975. The mammalian spermatozoon. Dev Biol **44:**394–436. http://dx.doi.org/10.1016/0012-1606(75)90411-X.
18. **Griswold MD.** 1998. The central role of Sertoli cells in spermatogenesis. Semin Cell Dev Biol **9:**411–416. http://dx.doi.org/10.1006/scdb.1998.0203.
19. **Ramskold D, Wang ET, Burge CB, Sandberg R.** 2009. An abundance of ubiquitously expressed genes revealed by tissue transcriptome sequence data. PLoS Comput Biol **5:**e1000598. http://dx.doi.org/10.1371/journal.pcbi.1000598.
20. **Soumillon M, Necsulea A, Weier M, Brawand D, Zhang X, Gu H, Barthes P, Kokkinaki M, Nef S, Gnirke A, Dym M, de Massy B, Mikkelsen TS, Kaessmann H.** 2013. Cellular source and mechanisms of high transcriptome complexity in the mammalian testis. Cell Rep **3:**2179–2190. http://dx.doi.org/10.1016/j.celrep.2013.05.031.
21. **Kleene KC.** 2013. Connecting cis-elements and trans-factors with mechanisms of developmental regulation of mRNA translation in meiotic and haploid mammalian spermatogenic cells. Reproduction **146:**R1–R19. http://dx.doi.org/10.1530/REP-12-0362.
22. **Schmid R, Grellscheid SN, Ehrmann I, Dalgliesh C, Danilenko M, Paronetto MP, Pedrotti S, Grellscheid D, Dixon RJ, Sette C, Eperon IC, Elliott DJ.** 2013. The splicing landscape is globally reprogrammed during male meiosis. Nucleic Acids Res **41:**10170–10184. http://dx.doi.org/10.1093/nar/gkt811.
23. **Elliott DJ, Oghene K, Makarov G, Makarova O, Hargreave TB, Chandley AC, Eperon IC, Cooke HJ.** 1998. Dynamic changes in the subnuclear organisation of pre-mRNA splicing proteins and RBM during human germ cell development. J Cell Sci **111:**1255–1265.
24. **Xu M, Hecht NB.** 2007. Polypyrimidine tract binding protein 2 stabilizes phosphoglycerate kinase 2 mRNA in murine male germ cells by

binding to its 3′UTR. Biol Reprod **76:**1025–1033. http://dx.doi.org/10.1095/biolreprod.107.060079.
25. **Xu M, McCarrey JR, Hecht NB.** 2008. A cytoplasmic variant of the KH-type splicing regulatory protein serves as a decay-promoting factor for phosphoglycerate kinase 2 mRNA in murine male germ cells. Nucleic Acids Res **36:**7157–7167. http://dx.doi.org/10.1093/nar/gkn800.
26. **Lassalle B, Bastos H, Louis JP, Riou L, Testart J, Dutrillaux B, Fouchet P, Allemand I.** 2004. 'Side population' cells in adult mouse testis express Bcrp1 gene and are enriched in spermatogonia and germinal stem cells. Development **131:**479–487.
27. **Bastos H, Lassalle B, Chicheportiche A, Riou L, Testart J, Allemand I, Fouchet P.** 2005. Flow cytometric characterization of viable meiotic and postmeiotic cells by Hoechst 33342 in mouse spermatogenesis. Cytometry A **65:**40–49.
28. **Getun IV, Wu ZK, Khalil AM, Bois PR.** 2010. Nucleosome occupancy landscape and dynamics at mouse recombination hotspots. EMBO Rep **11:**555–560. http://dx.doi.org/10.1038/embor.2010.79.
29. **Lassalle B, Ziyyat A, Testart J, Finaz C, Lefevre A.** 1999. Flow cytometric method to isolate round spermatids from mouse testis. Hum Reprod **14:**388–394. http://dx.doi.org/10.1093/humrep/14.2.388.
30. **Takubo K, Ohmura M, Azuma M, Nagamatsu G, Yamada W, Arai F, Hirao A, Suda T.** 2008. Stem cell defects in ATM-deficient undifferentiated spermatogonia through DNA damage-induced cell-cycle arrest. Cell Stem Cell **2:**170–182. http://dx.doi.org/10.1016/j.stem.2007.10.023.
31. **Grisanti L, Falciatori I, Grasso M, Dovere L, Fera S, Muciaccia B, Fuso A, Berno V, Boitani C, Stefanini M, Vicini E.** 2009. Identification of spermatogonial stem cell subsets by morphological analysis and prospective isolation. Stem Cells **27:**3043–3052. http://dx.doi.org/10.1002/stem.206.
32. **Getun IV, Torres B, Bois PR.** 2011. Flow cytometry purification of mouse meiotic cells. J Vis Exp **2011**(50):2602. http://dx.doi.org/10.3791/2602.
33. **Smith L.** 2011. Good planning and serendipity: exploiting the Cre/Lox system in the testis. Reproduction **141:**151–161. http://dx.doi.org/10.1530/REP-10-0404.
34. **Sadate-Ngatchou PI, Payne CJ, Dearth AT, Braun RE.** 2008. Cre recombinase activity specific to postnatal, premeiotic male germ cells in transgenic mice. Genesis **46:**738–742. http://dx.doi.org/10.1002/dvg.20437.
35. **Hobbs RM, Fagoonee S, Papa A, Webster K, Altruda F, Nishinakamura R, Chai L, Pandolfi PP.** 2012. Functional antagonism between Sall4 and Plzf defines germline progenitors. Cell Stem Cell **10:**284–298. http://dx.doi.org/10.1016/j.stem.2012.02.004.
36. **Bellve AR, Cavicchia JC, Millette CF, O'Brien DA, Bhatnagar YM, Dym M.** 1977. Spermatogenic cells of the prepuberal mouse. Isolation and morphological characterization. J Cell Biol **74:**68–85.
37. **Obholz KL, Akopyan A, Waymire KG, MacGregor GR.** 2006. FNDC3A is required for adhesion between spermatids and Sertoli cells. Dev Biol **298:**498–513. http://dx.doi.org/10.1016/j.ydbio.2006.06.054.
38. **Faridha A, Faisal K, Akbarsha MA.** 2007. Aflatoxin treatment brings about generation of multinucleate giant spermatids (symplasts) through opening of cytoplasmic bridges: light and transmission electron microscopic study in Swiss mouse. Reprod Toxicol **24:**403–408. http://dx.doi.org/10.1016/j.reprotox.2007.04.071.
39. **Eddy EM.** 2002. Male germ cell gene expression. Recent Prog Horm Res **57:**103–128. http://dx.doi.org/10.1210/rp.57.1.103.
40. **Ahmed EA, de Rooij DG.** 2009. Staging of mouse seminiferous tubule cross-sections. Methods Mol Biol **558:**263–277. http://dx.doi.org/10.1007/978-1-60761-103-5_16.
41. **Berruti G, Paiardi C.** 2011. Acrosome biogenesis: revisiting old questions to yield new insights. Spermatogenesis **1:**95–98. http://dx.doi.org/10.4161/spmg.1.2.16820.
42. **Petersen TW, Ibrahim SF, Diercks AH, van den Engh G.** 2004. Chromatic shifts in the fluorescence emitted by murine thymocytes stained with Hoechst 33342. Cytometry A **60:**173–181.
43. **Watson JV, Nakeff A, Chambers SH, Smith PJ.** 1985. Flow cytometric fluorescence emission spectrum analysis of Hoechst-33342-stained DNA in chicken thymocytes. Cytometry **6:**310–315. http://dx.doi.org/10.1002/cyto.990060406.
44. **Smith PJ, Nakeff A, Watson JV.** 1985. Flow-cytometric detection of changes in the fluorescence emission spectrum of a vital DNA-specific dye in human tumour cells. Exp Cell Res **159:**37–46. http://dx.doi.org/10.1016/S0014-4827(85)80035-5.
45. **Vasileva A, Tiedau D, Firooznia A, Muller-Reichert T, Jessberger R.** 2009. Tdrd6 is required for spermiogenesis, chromatoid body architecture, and regulation of miRNA expression. Curr Biol **19:**630–639. http://dx.doi.org/10.1016/j.cub.2009.02.047.
46. **De Gasperi R, Rocher AB, Sosa MA, Wearne SL, Perez GM, Friedrich VLJ, Hof PR, Elder GA.** 2008. The IRG mouse: a two-color fluorescent reporter for assessing Cre-mediated recombination and imaging complex cellular relationships in situ. Genesis **46:**308–317. http://dx.doi.org/10.1002/dvg.20400.
47. **Gaysinskaya V, Soh IY, van der Heijden GW, Bortvin A.** 2014. Optimized flow cytometry isolation of murine spermatocytes. Cytometry A **85:**556–565. http://dx.doi.org/10.1002/cyto.a.22463.
48. **Bao J, Ma HY, Schuster A, Lin YM, Yan W.** 2013. Incomplete cre-mediated excision leads to phenotypic differences between Stra8-iCre; Mov10l1(lox/lox) and Stra8-iCre; Mov10l1(lox/Delta) mice. Genesis **51:**481–490. http://dx.doi.org/10.1002/dvg.22389.
49. **McCarrey JR, Berg WM, Paragioudakis SJ, Zhang PL, Dilworth DD, Arnold BL, Rossi JJ.** 1992. Differential transcription of Pgk genes during spermatogenesis in the mouse. Dev Biol **154:**160–168. http://dx.doi.org/10.1016/0012-1606(92)90056-M.
50. **Licatalosi DD, Darnell RB.** 2010. RNA processing and its regulation: global insights into biological networks. Nat Rev Genet **11:**75–87. http://dx.doi.org/10.1038/nrg2673.
51. **Ellis JD, Barrios-Rodiles M, Colak R, Irimia M, Kim T, Calarco JA, Wang X, Pan Q, O'Hanlon D, Kim PM, Wrana JL, Blencowe BJ.** 2012. Tissue-specific alternative splicing remodels protein-protein interaction networks. Mol Cell **46:**884–892. http://dx.doi.org/10.1016/j.molcel.2012.05.037.
52. **Buljan M, Chalancon G, Eustermann S, Wagner GP, Fuxreiter M, Bateman A, Babu MM.** 2012. Tissue-specific splicing of disordered segments that embed binding motifs rewires protein interaction networks. Mol Cell **46:**871–883. http://dx.doi.org/10.1016/j.molcel.2012.05.039.
53. **Chen WS, Xu PZ, Gottlob K, Chen ML, Sokol K, Shiyanova T, Roninson I, Weng W, Suzuki R, Tobe K, Kadowaki T, Hay N.** 2001. Growth retardation and increased apoptosis in mice with homozygous disruption of the Akt1 gene. Genes Dev **15:**2203–2208. http://dx.doi.org/10.1101/gad.913901.
54. **MacGregor GR, Russell LD, Van Beek ME, Hanten GR, Kovac MJ, Kozak CA, Meistrich ML, Overbeek PA.** 1990. Symplastic spermatids (sys): a recessive insertional mutation in mice causing a defect in spermatogenesis. Proc Natl Acad Sci U S A **87:**5016–5020. http://dx.doi.org/10.1073/pnas.87.13.5016.
55. **van der Weyden L, Arends MJ, Chausiaux OE, Ellis PJ, Lange UC, Surani MA, Affara N, Murakami Y, Adams DJ, Bradley A.** 2006. Loss of TSLC1 causes male infertility due to a defect at the spermatid stage of spermatogenesis. Mol Cell Biol **26:**3595–3609. http://dx.doi.org/10.1128/MCB.26.9.3595-3609.2006.
56. **Yamada D, Yoshida M, Williams YN, Fukami T, Kikuchi S, Masuda M, Maruyama T, Ohta T, Nakae D, Maekawa A, Kitamura T, Murakami Y.** 2006. Disruption of spermatogenic cell adhesion and male infertility in mice lacking TSLC1/IGSF4, an immunoglobulin superfamily cell adhesion molecule. Mol Cell Biol **26:**3610–3624. http://dx.doi.org/10.1128/MCB.26.9.3610-3624.2006.
57. **Bi J, Li Y, Sun F, Saalbach A, Klein C, Miller DJ, Hess R, Nowak RA.** 2013. Basigin null mutant male mice are sterile and exhibit impaired interactions between germ cells and Sertoli cells. Dev Biol **380:**145–156. http://dx.doi.org/10.1016/j.ydbio.2013.05.023.
58. **Batista F, Lu L, Williams SA, Stanley P.** 2012. Complex N-glycans are essential, but core 1 and 2 mucin O-glycans, O-fucose glycans, and NOTCH1 are dispensable, for mammalian spermatogenesis. Biol Reprod **86:**179. http://dx.doi.org/10.1095/biolreprod.111.098103.
59. **Yuan W, Leisner TM, McFadden AW, Clark S, Hiller S, Maeda N, O'Brien DA, Parise LV.** 2006. CIB1 is essential for mouse spermatogenesis. Mol Cell Biol **26:**8507–8514. http://dx.doi.org/10.1128/MCB.01488-06.
60. **Hellsten E, Bernard DJ, Owens JW, Eckhaus M, Suchy SF, Nussbaum RL.** 2002. Sertoli cell vacuolization and abnormal germ cell adhesion in mice deficient in an inositol polyphosphate 5-phosphatase. Biol Reprod **66:**1522–1530. http://dx.doi.org/10.1095/biolreprod66.5.1522.
61. **Kyronlahti A, Euler R, Bielinska M, Schoeller EL, Moley KH, Toppari J, Heikinheimo M, Wilson DB.** 2011. GATA4 regulates Sertoli cell function and fertility in adult male mice. Mol Cell Endocrinol **333:**85–95. http://dx.doi.org/10.1016/j.mce.2010.12.019.